Aircraft ice-nucleating particle and aerosol composition measurements in the Western North American Arctic

Alberto Sanchez-Marroquin[1], Sarah L. Barr [1], Ian T. Burke[1], James B. McQuaid[1], Benjamin J. Murray[1] (*)

[1]School of Earth and Environment, University of Leeds, Woodhouse Lane, Leeds, LS2 9JT, UK

(*) Corresponding author: b.j.murray@leeds.ac.uk

Knowledge of the temperature dependent concentration of ice-nucleating particles (INPs) is crucial to understanding the properties of mixed-phase clouds. However, the sources, transport and removal of INPs around the globe, and particularly in the Arctic region, are poorly understood. In the Arctic winter and spring, when many local sources are covered by ice and snow, it is not clear which INP types are important. In this study, we present a new dataset of aircraft-based immersion mode INP measurements and aerosol size-resolved composition in the Western North American Arctic from the 11th – 21st March 2018. Aerosol samples were collected on filters that were analysed using both a freezing droplet-based assay and Scanning Electron Microscopy with Energy Dispersive Spectroscopy (SEM-EDS). The measured INP concentrations were at or close to the limit of detection, with concentrations at -20°C of 1 L^{-1} or below. The size-resolved composition measurements indicates that the aerosol concentrations were low, dominated mostly by sea spray aerosol and mineral dust. Further analysis shows that mineral dust is important for the ice-nucleating properties of our samples, dominating over the sea spray aerosol particles in the four cases we analysed, suggesting that mineral dust is a relevant source of INPs in the Alaskan Arctic. Furthermore, the INP concentrations are more consistent with fertile soil dusts that have an ice active biological component than what would be expected for the ice-active mineral K-feldspar alone. While we cannot rule out local high latitude sources of dust, the relatively small size of the mineral dust implies that the dust was from distant sources.

1. Introduction

Clouds containing both supercooled liquid water and ice are known as mixed-phase clouds and they reflect a substantial amount of the incoming solar shortwave radiation that reaches the Earth (Boucher, 2013). The lifetime, as well as the amount of radiation that these clouds reflect, is strongly affected by the partitioning between liquid and ice (Storelvmo et al., 2015). When above temperatures required for homogeneous freezing (below ~-35°C), ice formation in mixed-phase clouds is initiated by the presence of a small fraction of the aerosol particles known as ice-nucleating particles (INPs) (Murray et al., 2012). Once ice crystals nucleate, they can grow more rapidly than liquid cloud droplets since ice has a lower equilibrium vapour pressure than supercooled water. This process can lead to the precipitation of the ice crystals, removing liquid water from a cloud (Korolev et al., 2017;Vergara-Temprado et al., 2018;Hawker et al., 2021). Ice-related processes in mixed-phase clouds such as the primary production of ice and the link to INP concentration are commonly oversimplified in climate models, which contributes to large discrepancies in the amount of water and ice that the models simulate (Komurcu et al., 2014;McCoy et al., 2016;McCoy et al., 2018). The difficulty of properly representing the current water and ice mixing state of these clouds is responsible for the large uncertainty of the cloud-phase feedback (Storelvmo et al., 2015). This negative cloud feedback is associated with phase changes in

46 mixed-phase clouds produced by a warming atmosphere (Ceppi et al., 2017;Murray et al., 2021). As
47 the atmosphere warms, mixed-phase clouds will contain more supercooled water and therefore have a
48 greater albedo, leading to a reduction in shortwave radiation reaching the surface. This is particularly
49 important for boundary layer cold sector clouds in the oceanic mid- to high-latitudes. Hence, better
50 understanding the sources and concentrations of atmospheric INPs, particularly at the mid- to high-
51 latitudes could help to reduce the uncertainty associated with cloud-phase feedback.

52 Only a small fraction of aerosol particles have the potential to become INPs. Transported dust from the
53 deserts is one of the most important sources of worldwide atmospheric INPs, especially at temperatures
54 below -15 °C (Hoose and Mohler, 2012;Vergara-Temprado et al., 2017;Kanji et al., 2017). Given the
55 fact that substantial amounts of dust are transported from the deserts to the Arctic (Fan, 2013;Huang et
56 al., 2015;Francis et al., 2018), this dust could contribute to the INP population of the region (Irish et al.,
57 2019;Yun et al., 2022). Additionally, local sources of high-latitude dust are known to contribute to the
58 dust budget in the Arctic (Bullard et al., 2016;Groot Zwaaftink et al., 2016;Meinander et al., 2021;Shi
59 et al., 2021). Some of these sources of high-latitude dust have been found to contribute to the Arctic
60 INP population (Tobo et al., 2019;Sanchez-Marroquin et al., 2020;Si et al., 2019). A fraction the INP
61 in the Arctic are also of biogenic origin (Wex et al., 2019;Porter et al., 2022), some of which may be
62 associated with biogenic material in sea spray and some of which may be from terrestrial sources
63 (Wilson et al., 2015;DeMott et al., 2016;Vergara-Temprado et al., 2017;Irish et al., 2017;McCluskey et
64 al., 2018;Bigg and Leck, 2001;Creamean et al., 2019;Hartmann et al., 2020). Other types of aerosol
65 particles such as volcanic ash or biomass burning particles could also contribute to the INP population
66 in the Arctic (Prenni et al., 2009).

67 The available literature data indicates that the INP concentrations in the Arctic are highly variable,
68 depending on the season and location (Murray et al., 2021). Wex et al. (2019) found that Arctic INP
69 concentrations reach a minimum during winter, but they increase through spring and reach a maximum
70 around the summer, suggesting that concentrations are highest when the transport of aerosol from the
71 low latitudes is at its weakest (the summer). Creamean et al. (2018) found a similar trend over spring,
72 with coarse particles being responsible for the higher INP concentration event. However, a recent study
73 did not find that seasonality of Arctic INPs (Rinaldi et al., 2021). Although substantial amounts of
74 anthropogenic pollutants exist in the Arctic during the spring, they do not seem to significantly
75 contribute to the INP concentration (Creamean et al., 2018;Borys, 1989). Measurements at the
76 summertime North Pole indicate highly variable INP concentrations, with air masses that have spent
77 the preceding week or so over ice-covered surfaces having very low INP particle concentrations, and
78 air masses originating from lower latitude ice-free regions along the Russian coast having very high
79 biological INP concentrations (Porter et al., 2022).

80 In this paper, we present a set of immersion mode INP and aerosol size-resolved composition
81 measurements carried out in the Western North American Arctic during March 2018. INP
82 measurements were combined with aerosol characteristics determined using SEM-EDS to indicate the
83 types of INPs that are were most important during this campaign.

84

2. Sampling location and methods

Aerosol particles were sampled from the UK's BAe-146 FAAM atmospheric research aircraft during the Measurements of Arctic Cloud, Snow and Sea Ice in the Marginal Ice ZonE (MACSSIMIZE) campaign, based in Fairbanks, Alaska (US) in March 2018. The majority of the measurements were carried out close to the northern coast of Alaska and the Canadian territory of Yukon, both over land and over the Arctic Ocean, as shown in Fig. 1, where the approximated midpoint of the filter sampling run locations are shown with a star. Measurements were carried out at altitudes between 60 and 600 m above sea level, as detailed in Table A1 along with other pertinent information. Additionally, the Hybrid Single-Particle Lagrangian Integrated Trajectory (HYSPLIT) model was used to calculate five day back trajectories of sampled air masses (Stein et al., 2015;Rolph et al., 2017) and shown in Fig. 1. The back trajectories show that in most cases air masses remained near or over Alaska and northern Canada before sampling. For 13 of the 16 samples, the trajectories indicate that the air mostly stayed at altitudes below 1000 m above sea level in the five days prior to sampling. At the time of sampling, most of the sea and land surfaces were covered by sea ice or snow (Fig. 1), which most likely suppressed any local aerosol sources.

Aerosol particles were collected using the filter inlet system on board of the FAAM BAe-146, which has been characterised by Sanchez-Marroquin et al. (2019). The system allowed us to collect two aerosol samples in parallel: one on a polycarbonate filter and one on a Teflon filter. Teflon filters were used to perform a droplet-on-filter freezing assay to quantify the INP concentration, as described in detail in Price et al. (2018) and Sanchez-Marroquin et al. (2020) and first described by Schnell (1982). In the present study, this approach consisted of pipetting 2 μL pure water droplets on to filters that had been exposed to aerosol particles. The filters were placed on top of a cold stage, within a chamber that is flushed with dry nitrogen gas to prevent water condensation, that is cooled at a constant rate. Droplet freezing was recorded and the resulting videos were analysed to determine the fraction of droplets frozen at each temperature and then the INP concentration. At least one handling blank experiment was performed for every flight. Handling blank filters were prepared and transported in the same way as the measurement filters including loading the filters into the sampling system on the aircraft and briefly opening (for a second or so) and closing the inlet valves that allow air to pass through the filters. Hence, the handling blank should provide information on sources of contamination throughout the handling of the filter. The majority of the samples were analysed a matter of hours after collection, however where this was not possible they were stored at ~ -18 ºC prior to analysis.

A subset of the polycarbonate filters was analysed using Scanning Electron Microscopy with Energy Dispersive Spectroscopy (SEM-EDS) to study aerosol size-resolved composition. This technique can be used to obtain the morphological and chemical properties of individual aerosol particles within the sample. Each particle is then classified into a defined composition category. A more detailed description of the technique can be found in Sanchez-Marroquin et al. (2019).

3. INP concentrations in the Western North American Arctic

The droplet fraction frozen (the fraction of droplet that were frozen as a function of temperature) produced by our samples, along with those produced by the handling blank filters, is shown in Fig 2a. While the fraction frozen for the sample filters were generally shifted to warmer temperatures than the handling blanks, many of the samples overlapped with the range defined by the handling blanks. Hence it was necessary to account for influence of the background from the measurements. The background subtraction procedure and the INP concentration calculations are detailed in Appendix B. Briefly, we converted our cumulative fraction frozen values for the samples and handling blanks into the differential INP spectrum, $k(T)$, in units of INP per unit temperature (Vali, 1971;Vali, 2019). k is the number of INP that become active in a temperature interval. This allowed us to define a limit of detection then

132   apply a criterion to separate samples that show a significant signal above this from the ones that do not.
133   Data points that were separated from the limit of detection by more than the error bar were considered
134   to be above the limit of detection. The error bars of the differential concentrations of the samples
135   represent a confidence level of 68 % while the error bars of the background represents the standard
136   deviation of all the measured handling blanks. Background-subtraction was applied to data points above
137   the limit of detection($k_{\mathrm{sample}} - k_{\mathrm{background}}$) using a similar approach to (Vali, 2019). The cumulative INP
138   spectrum, the common way of presenting INP data, was then derived using the background corrected
139   values of k.

140   The background corrected cumulative INP concentrations are shown in Fig 2b. Hollow markers indicate
141   measurements consistent with the limit of detection, where the lower error bar goes to zero, while filled
142   markers correspond to a cumulative INP concentration above the limit of detection. Approximately 70
143   % of the differential spectra binned data was not significantly above the limit of detection and around
144   half of the data points in the cumulative INP spectra shown in Fig. 2b show INP concentrations
145   consistent with zero (i.e. not above the detection limit). The reported INP concentrations are always
146   below 0.1 and 1 L^{-1} at – 15 $^{\circ}$C and -20 $^{\circ}$C, respectively. However, given the fact that a substantial
147   percentage of the data is not above the detection limit, the real values of some of these samples may be
148   well below these values. A daily, more detailed representation of the INP concentrations is shown in
149   Fig. B3.

150   INP concentrations across the Arctic vary significantly depending on the time of the year and location
151   (Creamean et al., 2018;Si et al., 2019;Wex et al., 2019). Hence, in order to compare to the pertinent
152   data we show our INP concentrations alongside literature data collected in a similar location and time
153   of the year in Fig. 3 (we restricted the literature datasets from February to April). Some of our reported
154   INP concentrations (full markers) are above some of the values measured by Creamean et al. (2018),
155   Wex et al. (2019) and Borys (1989). Creamean et al. (2018) reported INP concentrations at -20 $^{\circ}$C up
156   to 0.01 L^{-1} in a similar location in March. Measurements performed by Wex et al. (2019) in a close
157   location (Utqiaġvik) indicate that INP concentrations ranging from ~10^{-4} to 10^{-2} L^{-1} at -10 $^{\circ}$C in March.
158   The more active samples reported by Wex et al. (2019) form a consistent INP spectrum with our more
159   active samples, but unfortunately there is no direct overlap. Borys (1989) reported INP concentrations
160   of 0.001 L^{-1} to 0.3 L^{-1} at -25 $^{\circ}$C measured from an aircraft at a similar location and time of the year.
161   These values are of course consistent with our samples where we report upper limits, but some of our
162   samples clearly had substantially higher INP concentrations than the range reported by Borys (1989).
163   Although the literature INP concentrations have been measured in close locations at a similar time of
164   the year than the ones reported in this study, the measurements were performed in different years when
165   the INP population may have been different. Our measurements are still well within the range of
166   literature INP measurements from across the Arctic presented in Porter et al. (2022). Hence it seems
167   that during March 2018 the INP concentrations where sometimes higher in the Western North American
168   Arctic by about 1-2 orders of magnitude than defined by Creamean et al. and Borys et al., but are
169   consistent with the highest concentrations measured by Wex et al. (2019).

170

171   **4.   SEM-EDS size-resolved composition analysis**

172   The size distributions obtained with the SEM-EDS technique were compared with the size distributions
173   obtained using the optical particle counters, that measure the 0.1 to ~3 μm and ~3 to 50 μm ranges, on
174   board of the FAAM BAe-146 (Rosenberg et al., 2012;Sanchez-Marroquin et al., 2019). The analysis is
175   shown in Fig. 4 alongside the size-resolved chemical composition of the analysed samples.

176   The analysed samples exhibited low aerosol concentrations relative to other locations where we have
177   used this technique, especially for the coarse mode. In this study, almost no particles above 10 μm were
178   detected, in contrast to samples from other regions analysed using the same or similar technique, where

179 significant amounts of aerosols in between 10 and 20 µm were detected (Price et al., 2018;Sanchez-
180 Marroquin et al., 2019;Sanchez-Marroquin et al., 2020;Sanchez-Marroquin et al., 2021). Most of the
181 detected particles were below ~2 µm. At sizes below ~3 µm, the comparison between the optical probes
182 and the SEM-EDS size distributions are consistent in most cases, with an undercounting at the lower
183 end of the SEM-EDS technique (~0.3 µm). This undercounting is related to the difficulty in observing
184 small organic rich particles and has been discussed in Sanchez-Marroquin et al. (2019). At sizes above
185 ~3 µm, the optical probes and SEM-EDS size distributions showed a comparable amount of detected
186 particles in samples C089_3 and C090_1. However, for samples C087_1 and C091_2, the optical
187 counters detected a much larger concentration of particles with sizes ~5 to 10 µm. Furthermore, for
188 these two samples, the optical size distribution above ~3 µm has shape that is atypical of atmospheric
189 aerosol size distributions (the aerosol concentration drops about 4 orders of magnitude from ~5 to ~10
190 µm). As a consequence, it is very likely these parts of the size distribution measured by the optical
191 probes are produced by artefacts such as cloud droplets rather than representing the actual aerosol
192 concentration at that location.

193 In terms of chemical composition, the samples were mainly dominated by mineral dust and Na rich
194 particles. In this dataset, nearly all particles in the Na rich category were dominated by the presence of
195 Na and Cl, having traces of other elements (such as S in some occasions), consistent with sea spray
196 particles. As a consequence, we will refer to particles in this category as sea spray aerosol particles.
197 Some carbonaceous particles were also detected through most sizes and there were significant
198 contributions of S rich aerosol, particularly in the accumulation mode. As shown in Fig. 4 and Table 1,
199 the surface area of samples C087_1 and C091_2 were dominated by sea spray aerosol particles with
200 sizes around ~ 1 µm. In Fig. 1b it is shown that the air masses associated with these samples had been
201 circulating above the Arctic Ocean at relatively low altitude (below 500 m) before sampling took place.
202 This is consistent with the fact that sea spray aerosol particles are normally emitted by bubble bursting
203 in the surface of the oceans (Lewis and Schwartz, 2004). It is possible that the detected sea spray aerosol
204 was transported from ice free ocean masses. However, Fig. 1 indicates that the closest ocean masses
205 were almost fully covered by sea ice during the campaign and the majority of the sampled air masses
206 did not pass by the open oceans prior to sampling. Hence, it is also possible that the sea spray particles
207 had been emitted from open leads in the sea ice (Leck and Bigg, 1999;Kirpes et al., 2019), or directly
208 from the sea ice through blowing snow events (Yang et al., 2008;Huang and Jaeglé, 2017;Frey et al.,
209 2020).

210 Particles in the categories Si rich, Si only, Al-Si rich and Ca rich have a chemical composition consistent
211 with mineral dust particles so we will refer to them collectively as mineral dust. However, it should be
212 borne in mind that the composition of particles in these categories is also consistent with some types of
213 combustion ashes or volcanic ash. Mineral dust particles were present in all the samples, particularly
214 with sizes between 1 and 5 µm, constituting a substantial percentage of its surface area, as shown in
215 Table 1. This was particularly the case in the sample C090_1, where 56 % of the surface area was given
216 by mineral dust particles. Although we cannot fully determine the relative contribution of different
217 sources to the detected mineral dust, several arguments suggest that the sampled mineral dust originated
218 from the low latitude deserts. The back trajectory analysis shown in Fig. 1 suggests that most of the air
219 masses had been circulating around the sampling location prior to sampling for ~5 days. However, the
220 majority of the potential high-latitude dust sources were covered by snow at this time and mineral dust
221 originating from the Sahara and Central Asia is known to be transported to the Arctic in late winter and
222 early Spring, when this study took place (Fan, 2013;Huang et al., 2015;Francis et al., 2018).
223 Additionally, almost all the mineral dust particles found in this study had sizes below 5 µm. This
224 contrasts with results obtained using similar techniques on samples collected closer to dust sources,
225 where dust particles with sizes above 10 µm are frequent (Price et al., 2018;Ryder et al., 2018;Sanchez-
226 Marroquin et al., 2020). Although this evidence suggests that most of our dust likely originated in arid
227 lower-latitude deserts, high-latitude dust could still contribute to the dust budget or even dominate it
228 during other times of the year such as autumn (Groot Zwaaftink et al., 2016).

229 As shown in Table 1, C087_1 and C091_2 samples have a larger surface area of sea spray aerosol
230 particles (Na rich) than mineral dust, whereas sample C090_1 is dominated by the presence of mineral
231 dust. Hence, it is reasonable to ask if the mineral dust or organic material associated with sea spray is
232 the more important INP type in these samples. To estimate the relative contribution of mineral dust and
233 sea spray aerosol to the INP population, we present the expected INP concentrations based on the SEM-
234 EDS surface areas in Fig 3, in comparison with the measured INP concentrations. The INP
235 concentrations expected from the SEM-EDS analysis were calculated assuming a dust containing 10 %
236 of K-feldspar (Harrison et al., 2019) (the ice active component of desert dust) and the parametrization
237 of fertile soils given by O'Sullivan et al. (2014). Note that the latter is very similar to the desert dust
238 parameterization given by Ullrich et al. (2017). For the sea spray INP, the parametrization given by
239 McCluskey et al. (2018) that links INP concentration aerosol surface area has been used. As shown,
240 even in the cases where there is more sea spray aerosol than mineral dust (C087_1 and C091_2), the
241 minimum contribution of mineral dust INP is orders of magnitude above the INPs produced by the sea
242 spray aerosol particles. Additionally, the INP concentrations calculated based on the presence of dusts
243 better explains the observed INP concentrations measured using the droplet freezing assay at the lower
244 end of the temperature spectrum. At the higher end of the temperature spectrum, the measured INP
245 concentrations are above those expected from a 10 % K-feldspar dust, but are consistent with the fertile
246 soil dust parameterisation. It is known that fertile soil dusts contain biological ice nucleating material
247 (O'Sullivan et al., 2014), hence this suggests that the samples from Alaska contained some biological
248 ice nucleating material. Although our INP concentrations would also be comparable with those
249 predicted using the desert dust parameterization by Ullrich et al. (2017), the latter is usually higher than
250 the activity of samples of airborne desert dust at temperatures greater than about -20°C from other
251 studies (Boose et al., 2016;Price et al., 2018;Harrison et al., 2022;Reicher et al., 2018;Gong et al., 2020).
252 It has been suggested that dust that has been transported far from its source regions is less active than
253 arid soil dusts that have been recently aerosolised and also there appears to be substantial differences in
254 activity of dust from different source regions (Boose et al., 2016;Harrison et al., 2022). Hence, we
255 suggest that the enhanced ice-nucleation ability of our samples is due to the presence of biological
256 material. This is consistent with other studies, for example Wex et al. (2019) and Porter et al. (2022)
257 who also provides evidence that Arctic INP samples have a substantial biological component.

258
259 **5. Conclusions**

260 In this study, we present a new dataset of INP and SEM-EDS aerosol size-resolved composition
261 measurements in the Western North American Arctic in March 2018. Back trajectory analysis suggests
262 that these air masses spend the preceding five days circulating over or near Alaska and Northern Canada
263 where local sources of primary aerosol were supressed by snow and ice cover. Observed INP
264 concentrations were comparable or slightly higher than the limit of detection of the measuring
265 technique, being always below 0.1 and 1 L^{-1} at -15 °C and -20 °C respectively. SEM-EDS analysis
266 revealed that samples are mostly dominated by the presence of mineral dust and sea spray aerosol
267 particles, with some contributions of sulphur rich and carbonaceous particles. The mineral dust is most
268 likely sourced from the low-latitudes, rather than local high-latitude dust sources. Our analysis shows
269 that mineral dust will always contribute more INP to the INP population than sea spray, despite sea
270 spray being more abundant in some samples. However, it appears that the ice-active mineral K-Feldspar
271 cannot account for all of the observed INPs, especially above ~ -22°C. This suggests that there is another
272 INP type that controls the INP spectrum above -22°C; these particles may be biogenic in origin, but this
273 biogenic ice nucleating material might be derived from is unclear. More work is clearly required to
274 understand the sources and nature of INP in the winter and early spring Arctic.

Author contributions

Aerosol measurements during the MACSSIMIZE campaign were organised by ASM, JBM, and BJM. ASM and BJM worked on the manuscript with contributions from all authors. The field work was carried out by ASM and JBM. ASM performed all the experimental measurements (INP analysis and SEM-EDS). The SEM-EDS technique was developed by ASM and ITB. The back-trajectory analysis was carried out by SLB and ASM. All the authors contributed to the discussion.

Competing interests

The authors declare that they have no competing interests.

Data and materials availability

All data needed to evaluate the conclusions in the paper are present in the paper and/or the Supplementary Materials. The digitalized data are available from https://doi.org/xx.xxxx/xxx. FAAM data associated to the flights can be found in: Facility for Airborne Atmospheric Measurements; Natural Environment Research Council; Met Office (2018): FAAM C085 MACSSIMIZE flight: Airborne atmospheric measurements from core and non-core instrument suites on board the BAE-146 aircraft. Centre for Environmental Data Analysis. https://catalogue.ceda.ac.uk/uuid/b04281cc10c44d9dab1eb2e4eb19d5b8.
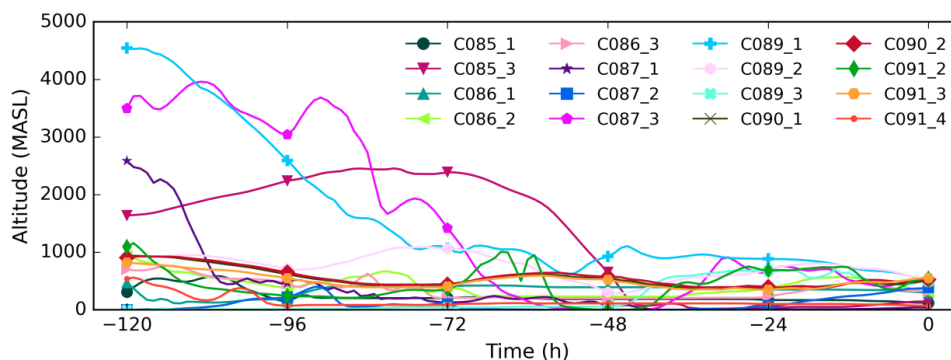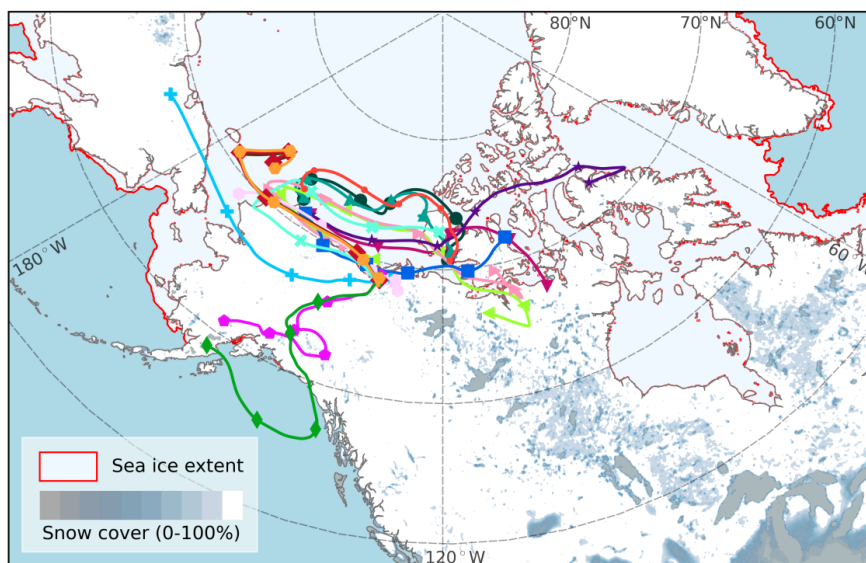
Figure 1. Map showing 5-day HYSPLIT back trajectories (upper panel) and altitude profile of each back trajectory (lower panel) from the midpoint of each sample location. The sampling location is marked using a star. The sea ice corresponds to 16th March 2018, extracted from the Multisensor Analyzed Sea Ice Extent - Northern Hemisphere (MASIE-NH) product at 1 km resolution (U.S. National Ice Center and National Snow and Ice Data Center. Compiled by F. Fetterer, 2010) . The snow cover corresponds to the average snow cover % for March 2018, extracted from ECMWF ERA5-Land monthly average reanalysis data (Muñoz Sabater, 2021).
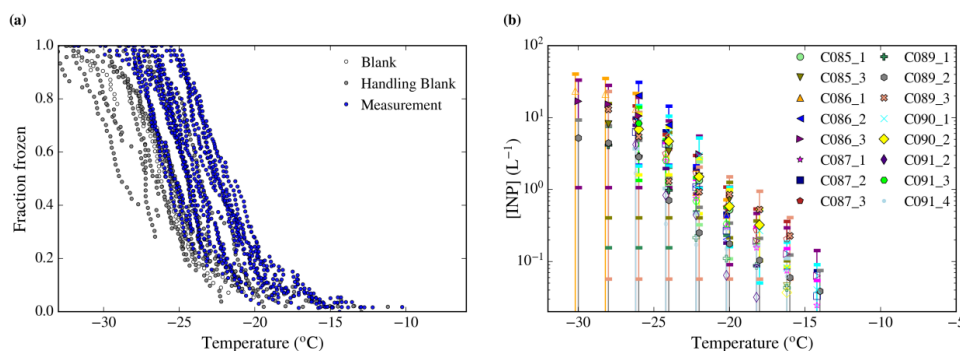
316
317 Figure 2. (a) Fraction of droplets frozen for all filter samples as well as blanks and handling blanks. (b)
318 INP particle concentrations for each filter sample. INP concentrations, upper limits and uncertainties
319 were calculated based on 68% confidence intervals, as shown in Appendix B. Data points corresponding
320 to the upper limits (open symbols) have been shifted 0.2 °C along the x-axis for clarity.

321
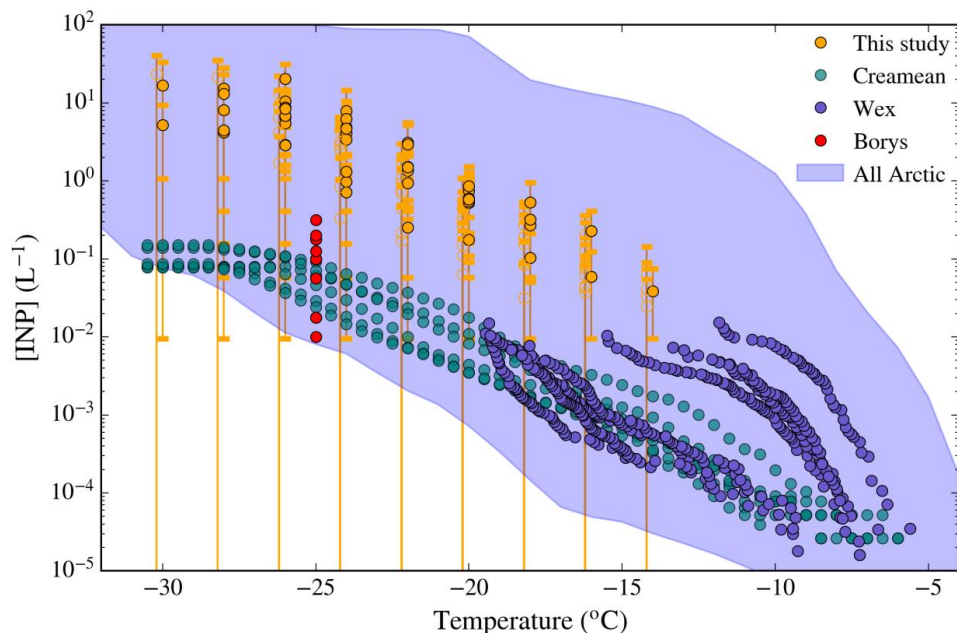
322
323 Figure 3. INP concentrations in this study compared with previous measurements at nearby locations
324 (Borys, 1989; Creamean et al., 2018; Wex et al., 2019). The background data range corresponds to the
325 range of literature INP Arctic measurements given by Porter et al. (2022). From the literature datasets,
326 only data collected from February, March and April have been shown as individual datasets. Note that
327 for the dataset of Wex et al. (2019), the concentrations increased through this period with the two highest
328 INP spectra from April. Also note that although the upper end of the literature Arctic measurement
329 range from Porter et al. (2022) corresponds to the highest concentrations ever recorded in the Arctic,
330 the majority of the Arctic concentrations fall in the lower half of the range. The points consistent with
331 the background (hollow symbols) is shown with slight offsets in temperature for greater clarity of the

332 error bars. The way in which the INP concentrations, upper limits and its uncertainties have been
333 calculated are shown in Appendix B, based on 68% confidence intervals.

334

335

336

337
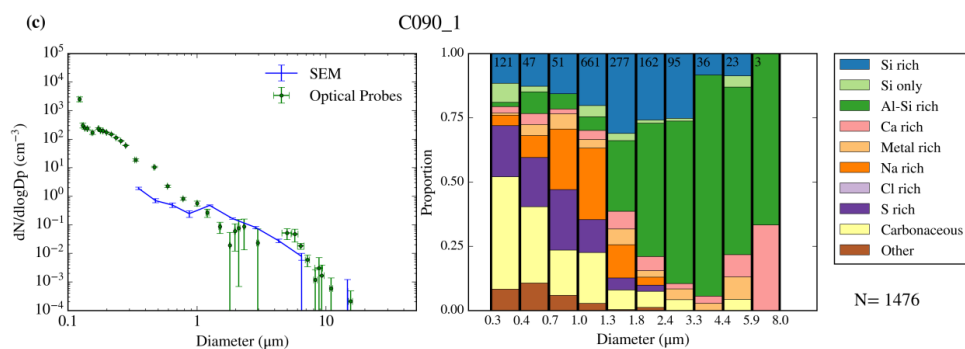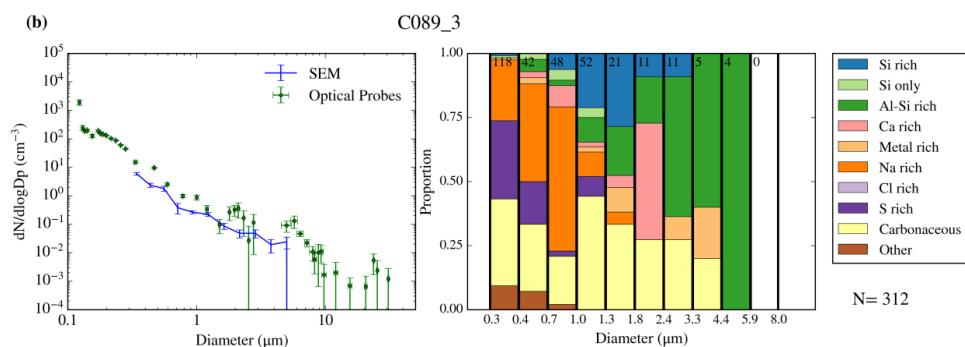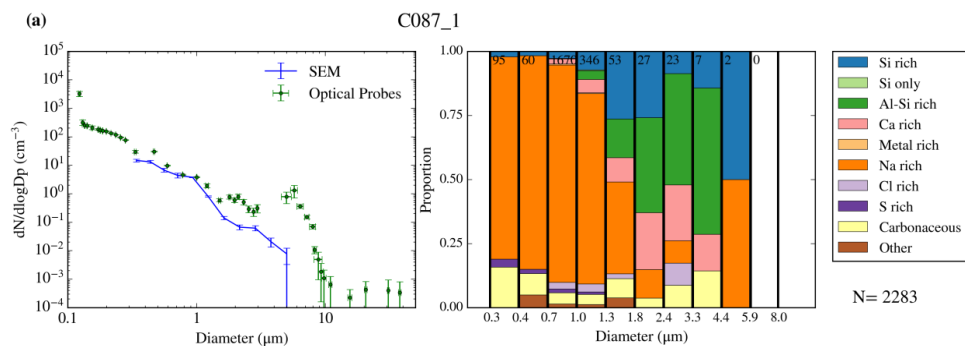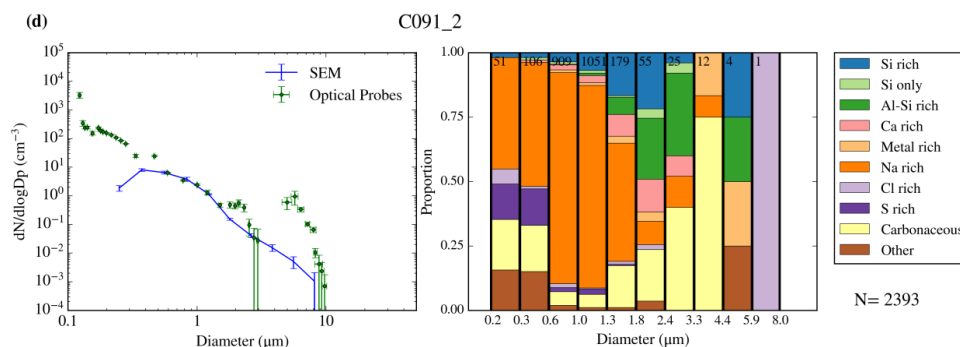
Figure 4. Results of SEM-EDS analysis of each analysed sample (a-d) showing comparison between SEM-EDS and PCASP-CDP number size distribution (left) alongside size-resolved composition (right).

Sample	Dust area (μm²/cm³)	Dust limit of detection (μm²/cm³)	Dust percentage	Sea spray aerosol area (μm²/cm³)	Sea spray aerosol percentage
C087_1	0.69	0.038	13.3	3.83	73.4
C089_3	0.66	0.15	43.9	0.28	18.8
C090_1	1.22	0.083	62.11	0.18	9.2
C091_2	0.53	0.049	11.1	2.86	60

Table 1. Surface area of dust and sea spray aerosol from SEM-EDS analysis. The dust limit of detection corresponds to the upper limit of the dust concentration detected on the handling blank filter. Note that the given dust and sea spray aerosol percentages refer to surface area percentages. The limit of detection of sea spray aerosol particles has not been indicated because the presence of this type of particles in the handling blank is negligible. Further information on the size-resolved composition of the handling blanks and a discussion about it can be found in (Sanchez-Marroquin et al., 2019).
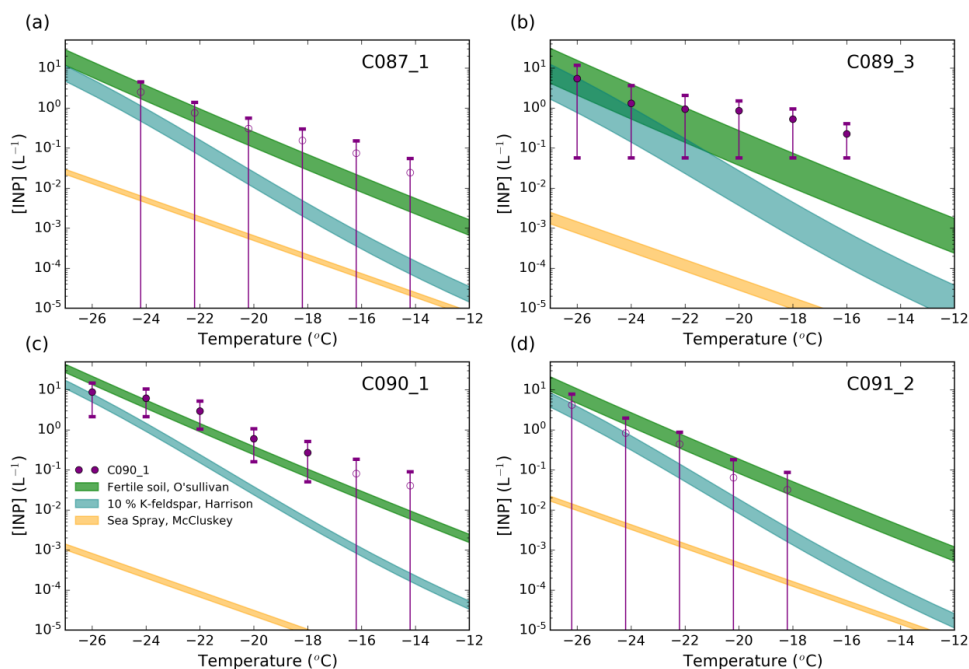
349
350 Figure 5. Predicted INP concentration of the SEM-EDS samples compared with the INP measurements
351 at -20 °C. The dust INP prediction has been calculated by applying different ice-nucleation
352 parametrizations to the surface area of dust calculated from the SEM-EDS analysis. The O'Sullivan et
353 al. (2014) for fertile soils and a dust containing 10 % of K-Feldspar (Harrison et al., 2019) have been
354 used. The NaCl INP prediction has been obtained by applying the sea spray aerosol parametrization
355 from McCluskey et al. (2018) to the SEM-EDS sea spray aerosol surface area. The purple points
356 correspond to our INP measurements or upper limits, based on 68% confidence intervals (Appendix B).

Appendix A: Sample details

Sample	Date (2017)	Start time (UTC)	End time (UTC)	Pressure altitude (m)	Radar altitude (m)	Vol. PC (L)	Vol. tef. (L)	PTFE position	Stored
C085_1	03/11th	22:22	22:34	496	474	466	312	Up	No
C085_3	03/11th	23:18	23:40	745	546	461	355	Low	No
C086_1	03/13th	21:14	21:22	36	38	212	159	Low	No
C086_2	03/13th	21:29	21:49	148	139	231	143	Up	No
C086_3	03/13th	22:11	22:31	421	387	644	209	Low	No
C087_1	03/16th	20:44	21:26	313	309	1047	565	Low	No
C087_2	03/16th	21:33	22:03	305	305	965	447	Up	No
C087_3	03/16th	22:30	22:44	547	491	392	217	Low	Yes
C089_1	03/18th	18:01	18:42	584	522	1198	714	Low	No
C089_2	03/18th	18:49	19:17	573	506	-	398	Low	No
C089_3	03/18th	19:28	19:48	596	557	404	214	Up	Yes
C090_1	03/20th	20:15	20:38	518	487	735	349	Low	No
C090_2	03/20th	20:53	21:26	518	487	488	409	Up	No
C091_2	03/21th	18:27	18:56	-72	123	1187	376	Up	No
C091_3	03/21th	19:01	19:14	130	297	644	203	Low	Yes
C091_4	03/21th	19:21	19:51	-138	68	635	635	Up	No

Table A1. Details of the samples collected during the MACSSIMIZE campaign. PTFE position refers to which inlet was used to collect the PTFE sample in each run. The other line was used to collect the polycarbonate sample. Stored filters were kept for a few hours or days at -18 °C, while the rest of them were analysed immediately after collection without any long-term storage.

Appendix B: Upper limit determination and background subtraction of the ice-nucleation experiments

As shown in Fig. 2a, most of the fraction of droplets frozen produced by the collected samples were comparable or only slightly above to the ones produced by the handling blanks. Hence, we established criteria to separate data points of the INP spectrum that are not significantly above the limit of detection of the instrument. The analysis is performed using the differential spectrum of ice-nucleus rather than the cumulative spectrum, which is normally used to display and compare ice-nucleation data such as INP concentrations and densities of active sites (Vali, 1971;Vali, 2019). First, we create a histogram with the number of freezing events per temperature interval per sample. This is done for all the samples and handling blanks, with temperature intervals of 2 °C. We transform the number of freezing events per interval of each sample into the differential INP spectrum, $k(T)$, using Eq. 1 (Vali, 2019).

$$k(T) = -\frac{1}{V \Delta T} ln \left(1 - \frac{\Delta N}{N(T)}\right)$$

Eq. 1

In Eq. 1, V is the droplet volume, ΔT is the temperature interval, ΔN is the number of frozen droplets between T and $(T-\Delta T)$, and $N(T)$ is the number of unfrozen droplets at T. The $k(T)$ values of the handling blanks is shown in Fig B1, alongside the mean value of each interval and its standard deviation. Note that many of the temperature intervals had zero freezing events, corresponding to k equal to zero. These zero values cannot be seen in Fig. B1 but they have been included in the means and standard deviations. The mean and standard deviation of the k values produced by each handling blank has been compared with the k values corresponding to each sample. The uncertainty in the k values associated with each sample has been calculated using a very similar Monte Carlo simulation as used previously (Vali, 2019) using a 68 % interval. The k values associated to each sample were individually compared with the mean and standard deviation of the k values of the handling blanks. A data point was considered above the limit of detection when its lower error yields above the mean plus standard deviation of the blanks. Background subtraction was applied to data points significantly above the limit of detection. This was done by subtracting the mean of the k values of the handling blanks. The error of the background-subtracted point was calculated by square rooting the quadratic sum of the error of the k_{sample} and $k_{background}$. Two examples of the comparisons between samples and the handling blanks are shown in Fig. B2. (a) corresponds to a case where no data point was higher than the limit of detection, while (b) corresponds to a case where most of the data points were significantly above the limit of detection. Note that all the data measured on the 16th of March (flight C087) has been flagged as an upper limit. This is because the handling blank experiment carried out on that day was unusually high, being compatible with all the measurements.

The background corrected $k(T)$ was integrated into the cumulative spectrum of active sites, $K(T)$, using Eq. 2 (Vali, 1971;Vali, 2019).

$$K(T) = \sum_{T=0}^{T} k(T) \Delta T$$

Eq. 2

INP concentrations were calculated from , $K(T)$ using Eq. 3, where V_d is the droplet volume, A_{filt} is the area of the filter, V_a is the sampled air volume and α is the contact surface of the droplets. For this study, we used the same values than Sanchez-Marroquin et al. (2021).

$$INP(T) = \frac{K(T)V_D A_{fil}}{V_a \alpha}$$

Eq. 3

A k value which was not significantly above the limit of detection has been represented with lower bars going to zero in the INP spectrum (meaning upper limit to the INP concentration). However, if a k value

403 not significantly above the limit of detection was preceded by a value which was above the limit of
404 detection, then as a result of the cumulative nature of the reported INP concentration the corresponding
405 value is reported with a filled symbol, but the lower bound of the error bar does not change since it is
406 possible that no new INP were present in that temperature interval. In Fig B3 one can see the INP
407 concentration of all the samples collected in this study per each day.

408
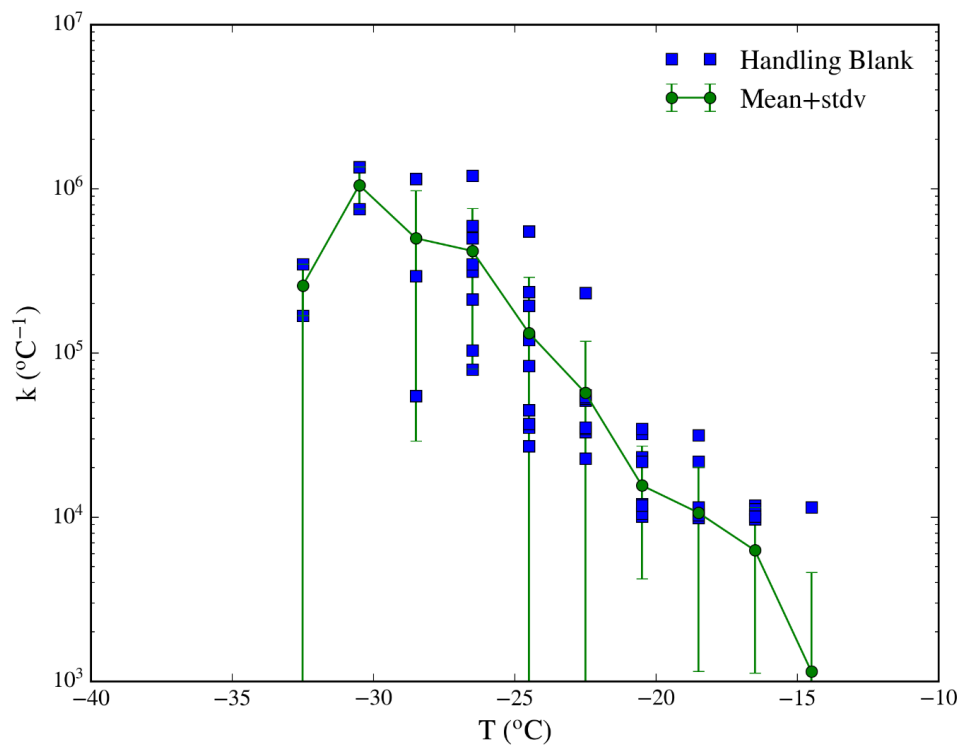
409

410 Figure B1. Differential spectrum of ice-nucleus of all the handling blanks performed during this
411 campaign. Data is shown in blue, while the mean and standard deviation of the data of each bin are
412 show in green.

413
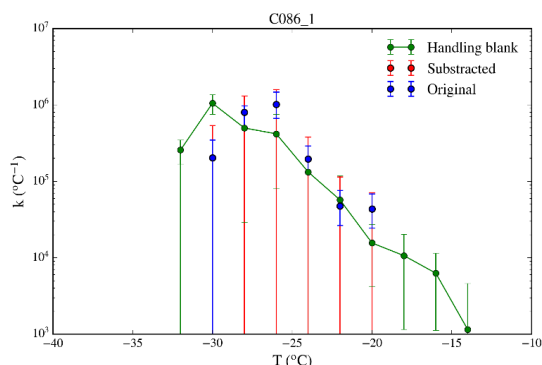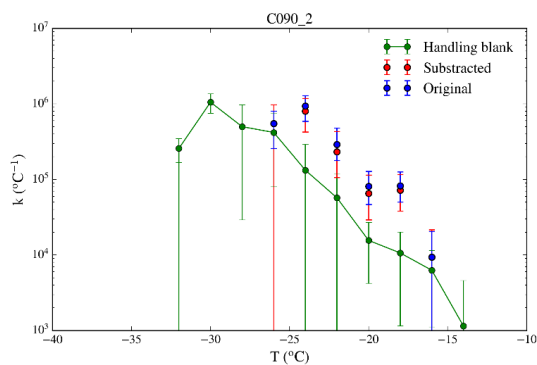
Figure B2. Examples of a comparison between the handling blank mean with two samples. None of the data points of sample C086_1 is significantly above the background. However, most of the data points associated with sample C090_2 are more than one error bar above the data produced by the handling blanks and they have been background-subtracted.
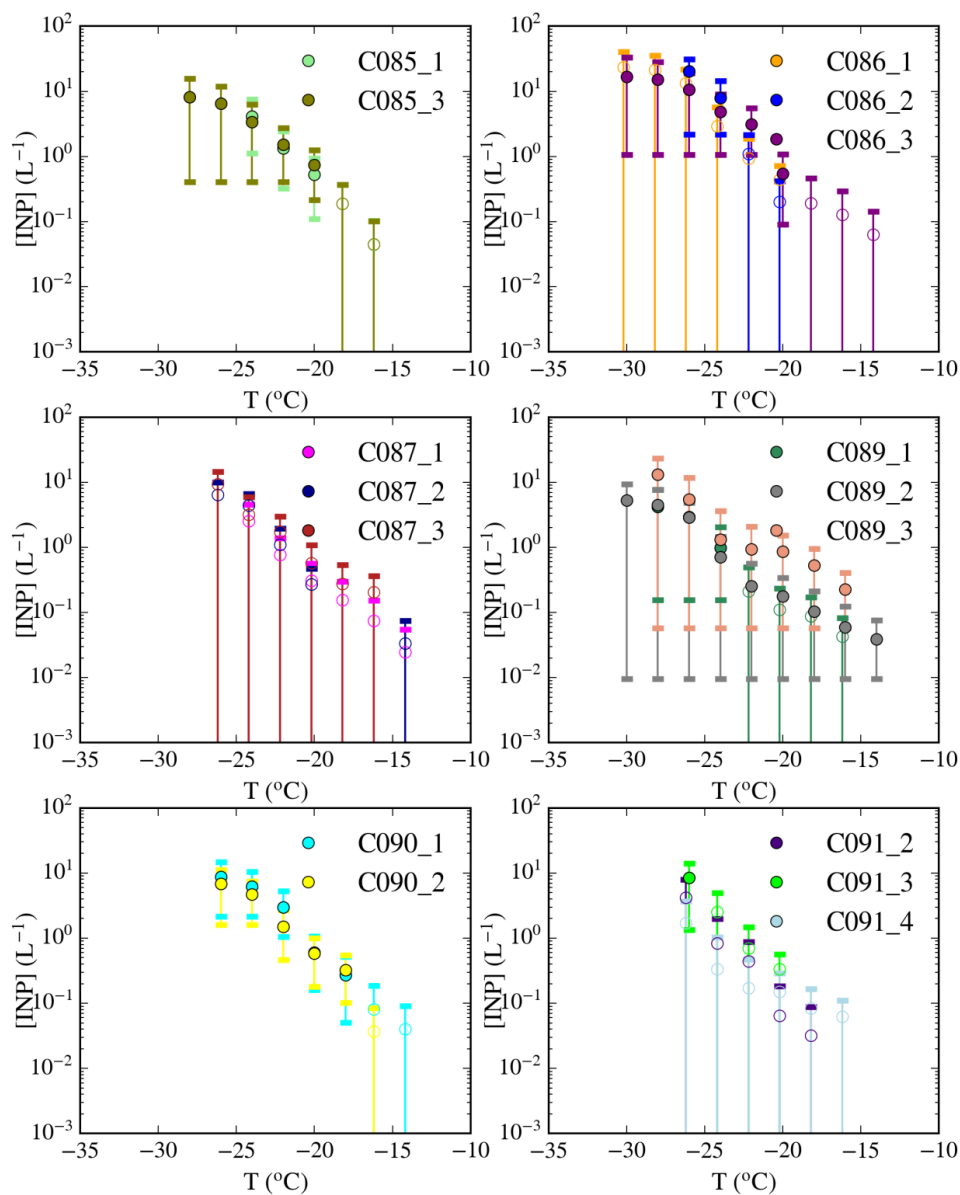
Fig B3. INP concentrations and upper limits shown in Fig. 2 separated per sampling day. A list of the days when these samples were collected is shown in Table A1.

References

Bigg, E. K., and Leck, C.: Cloud-active particles over the central Arctic Ocean, J. Geophys. Res. Atmos., 106, 32155-32166, 10.1029/1999jd901152, 2001.

Boose, Y., Sierau, B., García, M. I., Rodríguez, S., Alastuey, A., Linke, C., Schnaiter, M., Kupiszewski, P., Kanji, Z. A., and Lohmann, U.: Ice nucleating particles in the Saharan Air Layer, Atmos. Chem. Phys, 16, 9067-9087, 10.5194/acp-16-9067-2016, 2016.

Borys, R. D.: Studies of ice nucleation by Arctic aerosol on AGASP-II, J. Atmos. Chem., 9, 169-185, 10.1007/bf00052831, 1989.

Boucher, O., D. Randall, P. Artaxo, C. Bretherton, G. Feingold, P. Forster, V.-M. Kerminen, Y. Kondo, H. Liao, U. Lohmann, P. Rasch, S.K. Satheesh, S. Sherwood, B. Stevens and X.Y. Zhang, 2013: Climate Change 2013: The Physical Science Basis. Contribution of Working Group I to the Fifth Assessment Report of the Intergovernmental Panel on Climate Change, in, edited by: [Stocker, T. F., D. Qin, G.-K. Plattner, M. Tignor, S.K. Allen, J. Boschung, A. Nauels, Y. Xia, V. Bex and P.M. Midgley (eds.)], Cambridge University Press, Cambridge, United Kingdom and New York, NY, USA, 2013.

Bullard, J. E., Baddock, M., Bradwell, T., Crusius, J., Darlington, E., Gaiero, D., Gassó, S., Gisladottir, G., Hodgkins, R., McCulloch, R., McKenna-Neuman, C., Mockford, T., Stewart, H., and Thorsteinsson, T.: High-latitude dust in the Earth system, Rev Geophys, 54, 447-485, 10.1002/2016rg000518, 2016.

Ceppi, P., Brient, F., Zelinka, M. D., and Hartmann, D. L.: Cloud feedback mechanisms and their representation in global climate models, Wiley Interdisciplinary Reviews: Climate Change, 8, e465, 10.1002/wcc.465, 2017.

Creamean, J. M., Kirpes, R. M., Pratt, K. A., Spada, N. J., Maahn, M., de Boer, G., Schnell, R. C., and China, S.: Marine and terrestrial influences on ice nucleating particles during continuous springtime measurements in an Arctic oilfield location, Atmos. Chem. Phys, 18, 18023-18042, 10.5194/acp-18-18023-2018, 2018.

Creamean, J. M., Cross, J. N., Pickart, R., McRaven, L., Lin, P., Pacini, A., Hanlon, R., Schmale, D. G., Ceniceros, J., Aydell, T., Colombi, N., Bolger, E., and DeMott, P. J.: Ice Nucleating Particles Carried From Below a Phytoplankton Bloom to the Arctic Atmosphere, Geophys Res Lett, 46, 8572-8581, 10.1029/2019gl083039, 2019.

DeMott, P. J., Hill, T. C., McCluskey, C. S., Prather, K. A., Collins, D. B., Sullivan, R. C., Ruppel, M. J., Mason, R. H., Irish, V. E., Lee, T., Hwang, C. Y., Rhee, T. S., Snider, J. R., McMeeking, G. R., Dhaniyala, S., Lewis, E. R., Wentzell, J. J., Abbatt, J., Lee, C., Sultana, C. M., Ault, A. P., Axson, J. L., Diaz Martinez, M., Venero, I., Santos-Figueroa, G., Stokes, M. D., Deane, G. B., Mayol-Bracero, O. L., Grassian, V. H., Bertram, T. H., Bertram, A. K., Moffett, B. F., and Franc, G. D.: Sea spray aerosol as a unique source of ice nucleating particles, Proc Natl Acad Sci U S A, 113, 5797-5803, 10.1073/pnas.1514034112, 2016.

Fan, S.-M.: Modeling of observed mineral dust aerosols in the arctic and the impact on winter season low-level clouds, J. Geophys. Res. Atmos., 118, 11,161-111,174, 10.1002/jgrd.50842, 2013.

Francis, D., Eayrs, C., Chaboureau, J. P., Mote, T., and Holland, D. M.: Polar Jet Associated Circulation Triggered a Saharan Cyclone and Derived the Poleward Transport of the African Dust Generated by the Cyclone, J. Geophys. Res. Atmos., 123, 11,899-811,917, 10.1029/2018jd029095, 2018.

Frey, M. M., Norris, S. J., Brooks, I. M., Anderson, P. S., Nishimura, K., Yang, X., Jones, A. E., Nerentorp Mastromonaco, M. G., Jones, D. H., and Wolff, E. W.: First direct observation of sea salt aerosol production from blowing snow above sea ice, Atmos. Chem. Phys, 20, 2549-2578, 10.5194/acp-20-2549-2020, 2020.

Gong, X., Wex, H., van Pinxteren, M., Triesch, N., Fomba, K. W., Lubitz, J., Stolle, C., Robinson, T. B., Müller, T., Herrmann, H., and Stratmann, F.: Characterization of aerosol particles at Cabo Verde close to sea level and at the cloud level – Part 2: Ice-nucleating particles in air, cloud and seawater, Atmos. Chem. Phys, 20, 1451-1468, 10.5194/acp-20-1451-2020, 2020.

Groot Zwaaftink, C. D., Grythe, H., Skov, H., and Stohl, A.: Substantial contribution of northern high-latitude sources to mineral dust in the Arctic, J. Geophys. Res. Atmos., 121, 13,678-613,697, 10.1002/2016jd025482, 2016.

Harrison, A. D., Lever, K., Sanchez-Marroquin, A., Holden, M. A., Whale, T. F., Tarn, M. D., McQuaid, J. B., and Murray, B. J.: The ice-nucleating ability of quartz immersed in water and its atmospheric importance compared to K-feldspar, Atmospheric Chemistry and Physics Discussions, 2019, 1-23, 10.5194/acp-2019-288, 2019.

Harrison, A. D., O'Sullivan, D., Adams, M. P., Porter, G. C. E., Blades, E., Brathwaite, C., Chewitt-Lucas, R., Gaston, C., Hawker, R., Krüger, O. O., Neve, L., Pöhlker, M. L., Pöhlker, C., Pöschl, U., Sanchez-Marroquin, A., Sealy, A., Sealy, P., Tarn, M. D., Whitehall, S., McQuaid, J. B., Carslaw, K. S., Prospero, J. M., and Murray, B. J.: The ice-nucleating activity of African mineral dust in the Caribbean boundary layer, Atmos. Chem. Phys. Discuss., 2022, 1-34, 10.5194/acp-2022-57, 2022.

Hartmann, M., Adachi, K., Eppers, O., Haas, C., Herber, A., Holzinger, R., Hünerbein, A., Jäkel, E., Jentzsch, C., Pinxteren, M., Wex, H., Willmes, S., and Stratmann, F.: Wintertime Airborne Measurements of Ice Nucleating Particles in the High Arctic: A Hint to a Marine, Biogenic Source for Ice Nucleating Particles, Geophys Res Lett, 47, 10.1029/2020gl087770, 2020.

Hawker, R. E., Miltenberger, A. K., Wilkinson, J. M., Hill, A. A., Shipway, B. J., Cui, Z., Cotton, R. J., Carslaw, K. S., Field, P. R., and Murray, B. J.: The temperature dependence of ice-nucleating particle concentrations affects the radiative properties of tropical convective cloud systems, Atmos. Chem. Phys, 21, 5439-5461, 10.5194/acp-21-5439-2021, 2021.

Hoose, C., and Mohler, O.: Heterogeneous ice nucleation on atmospheric aerosols: a review of results from laboratory experiments, Atmos. Chem. Phys, 12, 9817-9854, 10.5194/acp-12-9817-2012, 2012.

Huang, J., and Jaeglé, L.: Wintertime enhancements of sea salt aerosol in polar regions consistent with a sea ice source from blowing snow, Atmos. Chem. Phys, 17, 3699-3712, 10.5194/acp-17-3699-2017, 2017.

Huang, Z., Huang, J., Hayasaka, T., Wang, S., Zhou, T., and Jin, H.: Short-cut transport path for Asian dust directly to the Arctic: a case study, Environmental Research Letters, 10, 114018, 10.1088/1748-9326/10/11/114018, 2015.

Irish, V. E., Elizondo, P., Chen, J., Chou, C., Charette, J., Lizotte, M., Ladino, L. A., Wilson, T. W., Gosselin, M., Murray, B. J., Polishchuk, E., Abbatt, J. P. D., Miller, L. A., and Bertram, A. K.: Ice-nucleating particles in Canadian Arctic sea-surface microlayer and bulk seawater, Atmos. Chem. Phys, 17, 10583-10595, 10.5194/acp-17-10583-2017, 2017.

Irish, V. E., Hanna, S. J., Willis, M. D., China, S., Thomas, J. L., Wentzell, J. J. B., Cirisan, A., Si, M., Leaitch, W. R., Murphy, J. G., Abbatt, J. P. D., Laskin, A., Girard, E., and Bertram, A. K.: Ice nucleating particles in the marine boundary layer in the Canadian Arctic during summer 2014, Atmos. Chem. Phys, 19, 1027-1039, 10.5194/acp-19-1027-2019, 2019.

Kanji, Z. A., Ladino, L. A., Wex, H., Boose, Y., Burkert-Kohn, M., Cziczo, D. J., and Krämer, M.: Overview of Ice Nucleating Particles, Meteorological Monographs, 58, 1.1-1.33, 10.1175/amsmonographs-d-16-0006.1, 2017.

Kirpes, R. M., Bonanno, D., May, N. W., Fraund, M., Barget, A. J., Moffet, R. C., Ault, A. P., and Pratt, K. A.: Wintertime Arctic Sea Spray Aerosol Composition Controlled by Sea Ice Lead Microbiology, ACS Cent Sci, 5, 1760-1767, 10.1021/acscentsci.9b00541, 2019.

Komurcu, M., Storelvmo, T., Tan, I., Lohmann, U., Yun, Y., Penner, J. E., Wang, Y., Liu, X., and Takemura, T.: Intercomparison of the cloud water phase among global climate models, J. Geophys. Res. Atmos., 119, 3372-3400, 10.1002/2013jd021119, 2014.

Korolev, A., McFarquhar, G., Field, P. R., Franklin, C., Lawson, P., Wang, Z., Williams, E., Abel, S. J., Axisa, D., Borrmann, S., Crosier, J., Fugal, J., Krämer, M., Lohmann, U., Schlenczek, O., Schnaiter, M., and Wendisch, M.: Mixed-Phase Clouds: Progress and Challenges, Meteorological Monographs, 58, 5.1-5.50, 10.1175/amsmonographs-d-17-0001.1, 2017.

Leck, C., and Bigg, E. K.: Aerosol production over remote marine areas-A new route, Geophys Res Lett, 26, 3577-3580, 10.1029/1999gl010807, 1999.

Lewis, E., and Schwartz, S.: Sea Salt Aerosol Production: Mechanisms, Methods, Measurements and Models—A Critical Review, GMS, 152, 3719, 10.1029/GM152, 2004.

McCluskey, C. S., Ovadnevaite, J., Rinaldi, M., Atkinson, J. D., Belosi, F., Ceburnis, D., Marullo, S., Hill, T. C. J., Lohmann, U., Kanji, Z. A., O'Dowd, C., Kreidenweis, S. M., and DeMott, P. J.: Marine and Terrestrial Organic Ice-Nucleating Particles in Pristine Marine to Continentally Influenced Northeast Atlantic Air Masses, J. Geophys. Res. Atmos., 123, 6196-6212, 10.1029/2017jd028033, 2018.

McCoy, D. T., Tan, I., Hartmann, D. L., Zelinka, M. D., and Storelvmo, T.: On the relationships among cloud cover, mixed-phase partitioning, and planetary albedo in GCMs, Journal of Advances in Modeling Earth Systems, 8, 650-668, 10.1002/2015ms000589, 2016.

McCoy, D. T., Hartmann, D. L., and Zelinka, M. D.: Chapter 9 - Mixed-Phase Cloud Feedbacks, in: Mixed-Phase Clouds, edited by: Andronache, C., Elsevier, 215-236, 2018.

Meinander, O., Dagsson-Waldhauserova, P., Amosov, P., Aseyeva, E., Atkins, C., Baklanov, A., Baldo, C., Barr, S., Barzycka, B., Benning, L., Cvetkovic, B., Enchilik, P., Frolov, D., Gassó, S., Kandler, K., Kasimov, N., Kavan, J., King, J., Koroleva, T., Krupskaya, V., Kusiak, M., Laska, M., Lasne, J., Lewandowski, M., Luks, B., McQuaid, J., Moroni, B., Murray, B., Möhler, O., Nawrot, A., Nickovic, S., O'Neill, N., Pejanovic, G., Popovicheva, O., Ranjbar, K., Romanias, M., Samonova, O., Sanchez-Marroquin, A., Schepanski, K., Semenkov, I., Sharapova, A., Shevnina, E., Shi, Z., Sofiev, M., Thevenet, F., Thorsteinsson, T., Timofeev, M., Umo, N. S., Uppstu, A., Urupina, D., Varga, G., Werner, T., Arnalds, O., and Vukovic Vimic, A.: Newly identified climatically and environmentally significant high latitude dust sources, Atmos. Chem. Phys. Discuss., 2021, 1-74, 10.5194/acp-2021-963, 2021.

563 Muñoz Sabater, J.: ERA5-Land monthly averaged data from 1981 to present, in, edited by:
564 (CDS), C. C. C. S. C. S. C. D. S., 2021.

565 Murray, B. J., O'Sullivan, D., Atkinson, J. D., and Webb, M. E.: Ice nucleation by particles
566 immersed in supercooled cloud droplets, Chem Soc Rev, 41, 6519-6554,
567 10.1039/c2cs35200a, 2012.

568 Murray, B. J., Carslaw, K. S., and Field, P. R.: Opinion: Cloud-phase climate feedback and
569 the importance of ice-nucleating particles, Atmos. Chem. Phys, 21, 665-679, 10.5194/acp-21-
570 665-2021, 2021.

571 O'Sullivan, D., Murray, B. J., Malkin, T. L., Whale, T. F., Umo, N. S., Atkinson, J. D., Price,
572 H. C., Baustian, K. J., Browse, J., and Webb, M. E.: Ice nucleation by fertile soil dusts:
573 relative importance of mineral and biogenic components, Atmos. Chem. Phys, 14, 1853-
574 1867, 10.5194/acp-14-1853-2014, 2014.

575 Porter, G. C. E., Adams, M. P., Brooks, I. M., Ickes, L., Karlsson, L., Leck, C., Salter, M. E.,
576 Schmale, J., Siegel, K., Sikora, S. N. F., Tarn, M. D., Vüllers, J., Wernli, H., Zieger, P.,
577 Zinke, J., and Murray, B. J.: Highly Active Ice-Nucleating Particles at the Summer North
578 Pole, J. Geophys. Res. Atmos., 127, 28, 10.1029/2021jd036059, 2022.

579 Prenni, A. J., Demott, P. J., Rogers, D. C., Kreidenweis, S. M., McFarquhar, G. M., Zhang,
580 G., and Poellot, M. R.: Ice nuclei characteristics from M-PACE and their relation to ice
581 formation in clouds, Tellus B, 61, 436-448, 10.1111/j.1600-0889.2009.00415.x, 2009.

582 Price, H. C., Baustian, K. J., McQuaid, J. B., Blyth, A., Bower, K. N., Choularton, T., Cotton,
583 R. J., Cui, Z., Field, P. R., Gallagher, M., Hawker, R., Merrington, A., Miltenberger, A.,
584 Neely Iii, R. R., Parker, S. T., Rosenberg, P. D., Taylor, J. W., Trembath, J., Vergara-
585 Temprado, J., Whale, T. F., Wilson, T. W., Young, G., and Murray, B. J.: Atmospheric Ice-
586 Nucleating Particles in the Dusty Tropical Atlantic, J. Geophys. Res. Atmos., 123, 2175-
587 2193, 10.1002/2017jd027560, 2018.

588 Reicher, N., Segev, L., and Rudich, Y.: The WeIzmann Supercooled Droplets Observation on
589 a Microarray (WISDOM) and application for ambient dust, Atmos. Meas. Tech., 11, 233-
590 248, 10.5194/amt-11-233-2018, 2018.

591 Rinaldi, M., Hiranuma, N., Santachiara, G., Mazzola, M., Mansour, K., Paglione, M.,
592 Rodriguez, C. A., Traversi, R., Becagli, S., Cappelletti, D., and Belosi, F.: Ice-nucleating
593 particle concentration measurements from Ny-Ålesund during the Arctic spring–summer in
594 2018, Atmos. Chem. Phys, 21, 14725-14748, 10.5194/acp-21-14725-2021, 2021.

595 Rolph, G., Stein, A., and Stunder, B.: Real-time Environmental Applications and Display
596 sYstem: READY, Environ. Model. Software, 95, 210-228, 10.1016/j.envsoft.2017.06.025,
597 2017.

598 Rosenberg, P. D., Dean, A. R., Williams, P. I., Dorsey, J. R., Minikin, A., Pickering, M. A.,
599 and Petzold, A.: Particle sizing calibration with refractive index correction for light scattering
600 optical particle counters and impacts upon PCASP and CDP data collected during the Fennec
601 campaign, Atmos. Meas. Tech., 5, 1147-1163, 10.5194/amt-5-1147-2012, 2012.

602 Ryder, C. L., Marenco, F., Brooke, J. K., Estelles, V., Cotton, R., Formenti, P., McQuaid, J.
603 B., Price, H. C., Liu, D. T., Ausset, P., Rosenberg, P. D., Taylor, J. W., Choularton, T.,
604 Bower, K., Coe, H., Gallagher, M., Crosier, J., Lloyd, G., Highwood, E. J., and Murray, B. J.:
605 Coarse-mode mineral dust size distributions, composition and optical properties from AER-D

606   aircraft measurements over the tropical eastern Atlantic, Atmos. Chem. Phys, 18, 17225-
607   17257, 10.5194/acp-18-17225-2018, 2018.

608   Sanchez-Marroquin, A., Hedges, D. H. P., Hiscock, M., Parker, S. T., Rosenberg, P. D.,
609   Trembath, J., Walshaw, R., Burke, I. T., McQuaid, J. B., and Murray, B. J.: Characterisation
610   of the filter inlet system on the FAAM BAe-146 research aircraft and its use for size-resolved
611   aerosol composition measurements, Atmos. Meas. Tech., 12, 5741-5763, 10.5194/amt-12-
612   5741-2019, 2019.

613   Sanchez-Marroquin, A., Arnalds, O., Baustian-Dorsi, K. J., Browse, J., Dagsson-
614   Waldhauserova, P., Harrison, A. D., Maters, E. C., Pringle, K. J., Vergara-Temprado, J.,
615   Burke, I. T., McQuaid, J. B., Carslaw, K. S., and Murray, B. J.: Iceland is an episodic source
616   of atmospheric ice-nucleating particles relevant for mixed-phase clouds, Science Advances,
617   6, eaba8137, 10.1126/sciadv.aba8137, 2020.

618   Sanchez-Marroquin, A., West, L. S., Burke, I. T., McQuaid, J. B., and Murray, B. J.: Mineral
619   and biological ice-nucleating particles above the South East of the British Isles, 2021.

620   Schnell, R. C.: Airborne ice nucleus measurements around the Hawaiian Islands, J. Geophys.
621   Res., 87, 8886, 10.1029/JC087iC11p08886, 1982.

622   Shi, Y., Liu, X., Wu, M., Ke, Z., and Brown, H.: Relative Importance of High-Latitude Local
623   and Long-Range Transported Dust to Arctic Ice Nucleating Particles and Impacts on Arctic
624   Mixed-Phase Clouds, Atmos. Chem. Phys. Discuss., 2021, 1-57, 10.5194/acp-2021-621,
625   2021.

626   Si, M., Evoy, E., Yun, J., Xi, Y., Hanna, S. J., Chivulescu, A., Rawlings, K., Veber, D., Platt,
627   A., Kunkel, D., Hoor, P., Sharma, S., Leaitch, W. R., and Bertram, A. K.: Concentrations,
628   composition, and sources of ice-nucleating particles in the Canadian High Arctic during
629   spring 2016, Atmos. Chem. Phys, 19, 3007-3024, 10.5194/acp-19-3007-2019, 2019.

630   Stein, A. F., Draxler, R. R., Rolph, G. D., Stunder, B. J. B., Cohen, M. D., and Ngan, F.:
631   NOAA's HYSPLIT Atmospheric Transport and Dispersion Modeling System, Bulletin of the
632   American Meteorological Society, 96, 2059-2077, 10.1175/bams-d-14-00110.1, 2015.

633   Storelvmo, T., Tan, I., and Korolev, A. V.: Cloud Phase Changes Induced by CO2
634   Warming—a Powerful yet Poorly Constrained Cloud-Climate Feedback, Current Climate
635   Change Reports, 1, 288-296, 10.1007/s40641-015-0026-2, 2015.

636   Tobo, Y., Adachi, K., DeMott, P. J., Hill, T. C. J., Hamilton, D. S., Mahowald, N. M.,
637   Nagatsuka, N., Ohata, S., Uetake, J., Kondo, Y., and Koike, M.: Glacially sourced dust as a
638   potentially significant source of ice nucleating particles, Nat Geosci, 12, 253-+,
639   10.1038/s41561-019-0314-x, 2019.

640   U.S. National Ice Center and National Snow and Ice Data Center. Compiled by F. Fetterer,
641   M. S., S. Helfrich, and P. Clemente-Colón: Multisensor Analyzed Sea Ice Extent - Northern
642   Hemisphere (MASIE-NH) in, 1 ed., Boulder, Colorado USA. National Snow and Ice Data
643   Center, 2010.

644   Ullrich, R., Hoose, C., Mohler, O., Niemand, M., Wagner, R., Hohler, K., Hiranuma, N.,
645   Saathoff, H., and Leisner, T.: A New Ice Nucleation Active Site Parameterization for Desert
646   Dust and Soot, J. Atmospheric Sci., 74, 699-717, 10.1175/Jas-D-16-0074.1, 2017.

647   Vali, G.: Quantitative Evaluation of Experimental Results an the Heterogeneous Freezing
648   Nucleation of Supercooled Liquids, J. Atmospheric Sci., 28, 402-409, 10.1175/1520-
649   0469(1971)028<0402:QEOERA>2.0.CO;2, 1971.

650   Vali, G.: Revisiting the differential freezing nucleus spectra derived from drop-freezing
651   experiments: methods of calculation, applications, and confidence limits, Atmos. Meas.
652   Tech., 12, 1219-1231, 10.5194/amt-12-1219-2019, 2019.

653   Vergara-Temprado, J., Murray, B. J., Wilson, T. W., O'Sullivan, D., Browse, J., Pringle, K.
654   J., Ardon-Dryer, K., Bertram, A. K., Burrows, S. M., Ceburnis, D., DeMott, P. J., Mason, R.
655   H., O'Dowd, C. D., Rinaldi, M., and Carslaw, K. S.: Contribution of feldspar and marine
656   organic aerosols to global ice nucleating particle concentrations, Atmos. Chem. Phys, 17,
657   3637-3658, 10.5194/acp-17-3637-2017, 2017.

658   Vergara-Temprado, J., Miltenberger, A. K., Furtado, K., Grosvenor, D. P., Shipway, B. J.,
659   Hill, A. A., Wilkinson, J. M., Field, P. R., Murray, B. J., and Carslaw, K. S.: Strong control
660   of Southern Ocean cloud reflectivity by ice-nucleating particles, Proc Natl Acad Sci U S A,
661   115, 2687-2692, 10.1073/pnas.1721627115, 2018.

662   Wex, H., Huang, L., Zhang, W., Hung, H., Traversi, R., Becagli, S., Sheesley, R. J., Moffett,
663   C. E., Barrett, T. E., Bossi, R., Skov, H., Hünerbein, A., Lubitz, J., Löffler, M., Linke, O.,
664   Hartmann, M., Herenz, P., and Stratmann, F.: Annual variability of ice-nucleating particle
665   concentrations at different Arctic locations, Atmos. Chem. Phys, 19, 5293-5311,
666   10.5194/acp-19-5293-2019, 2019.

667   Wilson, T. W., Ladino, L. A., Alpert, P. A., Breckels, M. N., Brooks, I. M., Browse, J.,
668   Burrows, S. M., Carslaw, K. S., Huffman, J. A., Judd, C., Kilthau, W. P., Mason, R. H.,
669   McFiggans, G., Miller, L. A., Najera, J. J., Polishchuk, E., Rae, S., Schiller, C. L., Si, M.,
670   Vergara-Temprado, J., Whale, T. F., Wong, J. P., Wurl, O., Yakobi-Hancock, J. D., Abbatt, J.
671   P., Aller, J. Y., Bertram, A. K., Knopf, D. A., and Murray, B. J.: A marine biogenic source of
672   atmospheric ice-nucleating particles, Nature, 525, 234-238, 10.1038/nature14986, 2015.

673   Yang, X., Pyle, J. A., and Cox, R. A.: Sea salt aerosol production and bromine release: Role
674   of snow on sea ice, Geophys Res Lett, 35, 1-5, 10.1029/2008gl034536, 2008.

675   Yun, J., Evoy, E., Worthy, S. E., Fraser, M., Veber, D., Platt, A., Rawlings, K., Sharma, S.,
676   Leaitch, W. R., and Bertram, A.: Ice nucleating particles in the Canadian High Arctic during
677   the fall of 2018, Environmental Science: Atmospheres, 10.1039/d1ea00068c, 2022.
678